THE JOURNAL OF PHYSICAL CHEMISTRY B

Article

pubs.acs.org/JPCB

Molecular Dynamics Simulations of the Rotational and Translational Diffusion of a Janus Rod-Shaped Nanoparticle

Ali Kharazmi[†] and Nikolai V. Priezjev*[,‡,§]

[†]Department of Mechanical Engineering, Michigan State University, East Lansing, Michigan 48824, United States
[‡]Department of Mechanical and Materials Engineering, Wright State University, Dayton, Ohio 45435, United States
[§]National Research University Higher School of Economics, Moscow 101000, Russia

ABSTRACT: The diffusion of a Janus rod-shaped nanoparticle in a dense Lennard-Jones fluid is studied using molecular dynamics (MD) simulations. The Janus particle is modeled as a rigid cylinder whose atoms at each end have different interaction energies with fluid molecules, thus comprising wetting and nonwetting surfaces. We found that both rotational and translational diffusion coefficients are larger for Janus particles with lower average wettability, and these values are bound between the two limiting cases of uniformly wetting and nonwetting particles. It was also shown that values of the diffusion coefficients for displacements parallel and perpendicular to the major axis of a uniformly wetting particle agree well with analytical predictions despite a finite slip at the particle surface present in MD simulations. It was further demonstrated that diffusion of Janus particles is markedly different from that of uniform particles; namely, Janus particles preferentially rotate and orient their nonwetting ends along the displacement vector to reduce drag. This correlation between translation and rotation is consistent with the previous results on diffusive dynamics of a spherical Janus particle with two hemispheres of different wettability.

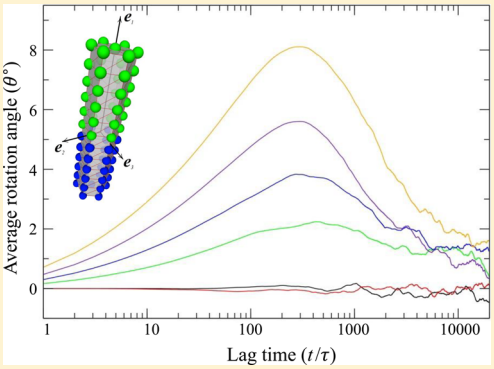

I. INTRODUCTION

The design of functional nanomaterials, with diverse applications in biomedicine, optoelectronics, and microfiltration, requires a detailed understanding of the diffusion process of anisotropic particles during their self-assembly in bulk fluid and at interfaces.[1−3] The synthesis of Janus nanoparticles often involves a masking step where particles are temporarily trapped at the interface between two phases and only one side can be treated chemically leading to asymmetric functionalization.[4] It was shown numerically that structural evolution of polymer blends can be significantly influenced by the orientation of Janus nanorods relative to the phase interface, and thus, it allows fabrication of polymer nanocomposites with robust photovoltaic and mechanical properties.[5,6] Common mechanisms of colloidal self-assembly include depletion-assisted structure formation, where effective forces between neighboring colloidal particles arise due to decreasing volume available to the depletant, and shape-complementary colloidal suspensions where only particles with matching building blocks bind together.[7] Interestingly, a variety of prescribed crystal or gel phases can be obtained via "programmable" self-assembly of DNA-grafted particles due to formation of bridges between neighboring particles.[8] Regardless of the specific interaction between particles, a complete picture of the diffusive motion even of isolated anisotropic particles is still missing.

The results of equilibrium molecular dynamics simulations have shown that the diffusion dynamics of a single spherical particle depends on its wetting properties, local boundary conditions, mass and size relative to the solvent molecules, as well as viscosity and temperature of the solvent.[9−17] Originally, it was discovered by Alder and Wainwright[18] that the velocity autocorrelation function exhibits a characteristic power-law decay at long times due to hydrodynamic coupling to the solvent. More recently, it was demonstrated that, in the presence of a liquid−solid interface, the power-law exponent is changed from the bulk value −3/2 to −5/2, while the amplitude of the velocity autocorrelation function increases for diffusive motion near the slipping boundary.[19,20] It was also shown that, as the particle size decreases down to a few molecular diameters, the Stokes−Einstein relation breaks down, and the effective radius of the particle might increase due to formation of an adjacent fluid layer if the surface energy is sufficiently large.[14] Despite significant computational efforts, the exact relationship between the local slip at confining boundaries and the position-dependent diffusion coefficient has yet to be established.

In recent years, various aspects of diffusive motion of a single Janus particle in the bulk and at liquid interfaces were studied using continuum[21−24] and molecular dynamics[25−28] simulations. In addition, a high-speed experimental technique to track translation and rotation of colloidal particles in three dimensions was recently developed and used to determine

Received: April 20, 2017
Revised: July 4, 2017
Published: July 17, 2017

DOI: 10.1021/acs.jpcb.7b03720
J. Phys. Chem. B 2017, 121, 7133−7139

accurately the diffusion coefficients of silica rods and spherical Janus particles in water.[29] Depending on the geometry of Janus particles (spherical, rod- or disk-like) and the degree of amphiphilicity, it was observed that particle rotational dynamics at sheared liquid−liquid interfaces involves either a smooth tilt or a tumbling motion.[27] In the previous study, the translational and rotational diffusion of a spherical Janus particle in a dense fluid was investigated using molecular dynamics simulations.[26] In particular, it was shown that Janus particles with lower surface energy diffuse faster, and their nonwetting hemispheres tend to orient along the displacement vector of the center of mass during the rotational relaxation time.[26] However, the combined effect of particle shape anisotropy and wettability contrast on diffusion remains not fully understood.

In this paper, we investigate the diffusion of a rod-shaped Janus particle in the limit of infinite dilution using molecular dynamics simulations. The particle consists of atoms rigidly fixed at the lattice sites that form a cylinder, which undergoes a diffusive motion under random forces from fluid molecules. In our model, the wall−fluid interaction energy at each end can be adjusted to control local wetting properties at the particle surface. We show that, with increasing wettability contrast, the translational and angular displacements become larger and the effective center of rotation is displaced toward the wetting end. We also demonstrate that a Janus particle on average is rotated by its nonwetting end along the displacement vector of the center of mass to reduce drag.

The paper is organized as follows. The details of the simulation procedure and the particle model are described in the next section. In section III, we report the fluid density profiles around particles, determine the local slip boundary conditions, and estimate translational and rotational diffusion coefficients from the particle trajectories and make a comparison with theoretical predictions. Brief conclusions are given in the last section.

II. SIMULATION METHOD

We use molecular dynamics simulations to study the translational and rotational diffusion of a single particle in an explicit solvent.[30] The model system consists of a rod-shaped Janus particle immersed in a monatomic fluid at equilibrium. A snapshot of the system is presented in Figure 1. In this model, any two fluid atoms interact via the truncated Lennard-Jones (LJ) potential as follows

$$V_{LJ}(r) = 4\varepsilon\left[\left(\frac{\sigma}{r}\right)^{12} - \left(\frac{\sigma}{r}\right)^{6}\right] \quad (1)$$

where the parameters ε and σ denote the energy and length scales of the fluid phase. For computational efficiency, the cutoff radius was set to $r_c = 2.5\sigma$ for fluid−fluid and fluid−solid interactions. The fluid phase consists of 46 536 monomers of mass m confined in a three-dimensional periodic cell with a linear side of 39.62σ. When the finite size of a Janus particle is taken into account, the uniform fluid density away from the particle is $\rho = 0.749\sigma^{-3}$. Periodic boundary conditions were applied in the $\hat{x}$, $\hat{y}$, and $\hat{z}$ directions. The MD simulations were carried out in the NVT ensemble, where the temperature, $T = 1.1\varepsilon/k_B$, was regulated by a Nosé−Hoover thermostat with a damping time of 1.0τ. Here, k_B is the Boltzmann constant. The equations of motion for fluid monomers and the Janus particle were solved using the Verlet integration algorithm[30,31] with a time step $\Delta t_{MD} = 0.005\tau$, where $\tau = \sigma\sqrt{m/\varepsilon}$ is the characteristic LJ time.

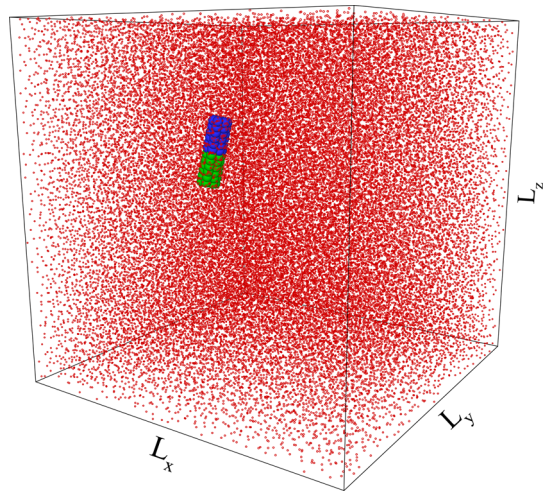

Figure 1. Snapshot of the rod-shaped Janus nanoparticle with wetting (blue atoms) and nonwetting (green atoms) ends and the surrounding Lennard-Jones fluid (red circles) in the periodic box with a linear size of 39.62σ. The number of fluid atoms is 46 536.

The Janus rod-shaped particle was constructed by arranging 72 atoms at vertices of 12 hexagons that are stacked together and by adding two atoms at both ends, as shown in Figure 2.

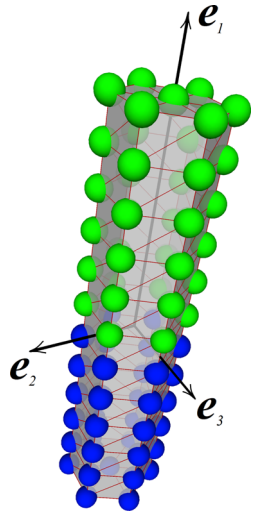

Figure 2. Janus particle consisting of 72 atoms fixed at the vertices of 12 stacked hexagons and two additional atoms at the outer faces. The blue atoms denote the wetting end, and the green atoms indicate the nonwetting end of the rod-shaped particle. The atoms are not drawn to scale. The reference frame of the particle is defined by the unit vectors $\mathbf{e}_1$, $\mathbf{e}_2$, and $\mathbf{e}_3$.

Hence, the particle consists of a total of 74 atoms that are fixed relative to each other and form a symmetric rod, which moves as a rigid body in the surrounding fluid. In this configuration, the distance between the outer hexagons along the $\mathbf{e}_1$ axis is 6.35σ and the hexagon side is 0.71σ, which is the same as the radius of a cylinder that contains all vertices. The size of all particles' atoms is the same as the size of fluid monomers. The interaction between solid atoms of the Janus particle and fluid monomers is also described by the LJ potential but with different energies. On the wetting side, the interaction energy is

DOI: 10.1021/acs.jpcb.7b03720
J. Phys. Chem. B 2017, 121, 7133−7139

fixed to $\varepsilon_{pf} = 1.0\varepsilon$, while, on the nonwetting side, ε_{pf} was varied from 0.1ε to 1.0ε. For reference, the cases of *uniformly* wetting and nonwetting particles were also considered, where the interaction energy with fluid monomers was set to $\varepsilon_{pf} = 1.0\varepsilon$ and $\varepsilon_{pf} = 0.1\varepsilon$, respectively. Finally, the total mass of the rod-shaped particle is fixed to $M = 50m$ in all simulations. The particle mass M was chosen to be much larger than the mass of a fluid monomer m in order to reduce backscattering effects at short times,[9,15] but on the other hand, this mass is small enough so that the particle can undergo large displacements in a dense fluid, leading to an accurate determination of diffusion coefficients without the need of excessive computational resources.

The large-scale molecular dynamics simulations were performed using the LAMMPS parallel code.[30] First, the system with the Janus particle and the fluid was equilibrated for 2×10^7 MD steps (or $10^5\tau$), followed by a production run of about 10^8 MD steps (or $0.5 \times 10^6\tau$). The data were gathered in 50 independent samples for uniform and Janus particles. For each sample, the position of the center of mass of the particle, its orientation vectors, as well as velocities and positions of all particle atoms were saved every 20 MD steps, and these data were used later for postprocessing.

III. RESULTS

We begin with a discussion of the fluid structure and local slip boundary conditions at the particle surface. The fluid density profiles around the nonwetting and wetting ends of Janus particles as well as around uniformly wetting and nonwetting particles are presented in Figure 3. The density profiles were

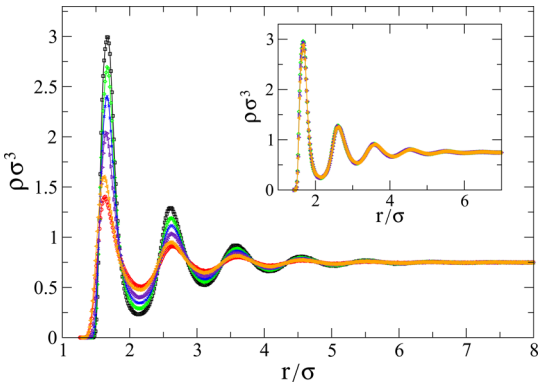

Figure 3. Radial fluid density profiles around the uniformly nonwetting particle with $\varepsilon_{pf} = 0.1\varepsilon$ (red), around the nonwetting end of Janus particles with $\varepsilon_{pf} = 0.1\varepsilon$ (orange), $\varepsilon_{pf} = 0.3\varepsilon$ (indigo), $\varepsilon_{pf} = 0.5\varepsilon$ (blue), $\varepsilon_{pf} = 0.7\varepsilon$ (green), and uniformly wetting particle with $\varepsilon_{pf} = 1.0\varepsilon$ (black). The inset shows the radial density profiles around the wetting end of Janus particles with the surface energy $\varepsilon_{pf} = 1.0\varepsilon$. The color code is the same.

averaged in thin cylindrical shells of radius r/σ around either wetting or nonwetting ends of Janus particles (see Figure 2). It can be seen in Figure 3 that in all cases the density profiles level off to the bulk value $\rho = 0.749\sigma^{-3}$ at $r \gtrsim 6\sigma$; however, a pronounced density layering is present at smaller distances, and the amplitude of density oscillations increases at larger surface energies. Notice that the height of the first peak appears to be slightly larger near the nonwetting end of the Janus particle with $\varepsilon_{pf} = 0.1\varepsilon$ than in the case of the uniformly nonwetting particle with the same surface energy because fluid monomers near the center of the Janus particle interact with atoms of the wetting end. In other words, the contact density of the adjacent fluid monomers varies gradually along the main axis of Janus particles due to the finite cutoff radius of the LJ potential and difference in surface energy at both ends. Correspondingly, the first peak in the density profiles around the wetting end of Janus particles is slightly smaller for larger wettability contrast, as shown in the inset of Figure 3. A similar effect of the contact density variation was observed in the previous MD studies of a spherical Janus particle in an explicit solvent[26] and liquid films confined by surfaces of patterned wettability.[32,33]

In order to determine the local flow boundary conditions at the particle surface, we carried out a set of MD simulations on a different system that consists of a monatomic fluid confined by smooth crystalline walls (but without Janus particles). The densities of the fluid phase and solid walls were chosen to be the same as that in the particle−fluid system described in the previous section. Special care was taken to match the nearest-neighbor distances between adjacent atoms at the particle surface (see Figure 2) and the lattice constants of the crystalline walls ($0.707\sigma \times 0.577\sigma$) that consist of a single plane each. The steady Poiseuille flow was induced by applying a small force, $f = 0.0005\varepsilon/\sigma$, to each fluid monomer in a direction parallel to the walls, while both walls remained at rest. As usual, the slip length was extracted from a parabolic fit to the velocity profile and then averaged over both interfaces.[34−36] The results are presented in Table 1. It can be seen that the slip length

Table 1. Variation of the Slip Length L_s/σ as a Function of the Wall−Fluid Interaction Energy Computed at Flat Interfaces between a Fluid Phase with the Density $\rho = 0.749\sigma^{-3}$ and Crystalline Surfaces with the Lattice Constants $0.707\sigma \times 0.577\sigma$ (See Text for Details)[a]

$\varepsilon_{pf}/\varepsilon$	0.1	0.3	0.5	0.7	1.0
L_s/σ	36.5	20.5	12.0	8.0	4.5

[a]The typical error bars for the slip length are about $\pm 1.0\sigma$.

increases for less wetting surfaces and it becomes larger than the particle size. We comment that this trend is expected to hold for atomically smooth interfaces when the wall−fluid interaction energy is sufficiently large.[37] We also remind that, in the presence of curved surfaces, the slip boundary condition is modified by the local radius of curvature.[38−41] Finally, the fluid viscosity was measured, $\eta = 1.66 \pm 0.03\varepsilon\tau\sigma^{-3}$, in steady flow at density $\rho = 0.749\sigma^{-3}$ and temperature $T = 1.1\varepsilon/k_B$.

It was previously shown that translational and rotational diffusion coefficients for a flat-end, rigid cylinder at short lag times can be approximated as follows

$$D_\perp \approx \frac{k_B T}{8\pi\eta b}(\ln \omega + 0.839 + 0.185/\omega + 0.233/\omega^2) \quad (2)$$

$$D_\parallel \approx \frac{k_B T}{4\pi\eta b}(\ln \omega - 0.207 + 0.980/\omega - 0.133/\omega^2) \quad (3)$$

$$D_r \approx \frac{3k_B T}{8\pi\eta b^3}(\ln \omega - 0.662 + 0.917/\omega - 0.050/\omega^2) \quad (4)$$

where $\omega = b/a$ is the aspect ratio, parameters a and b are the semiminor and semimajor axes of the cylinder, and η is the viscosity of the solvent.[29,42] These predictions are expected to hold at lag times smaller than the typical rotational relaxation time scale, since at larger lag times the orientation of the major axis of the cylinder is decorrelated from its initial direction and

DOI: 10.1021/acs.jpcb.7b03720
J. Phys. Chem. B 2017, 121, 7133−7139

the translational diffusion becomes isotropic. The interpolation equations, eqs 2−4, were derived for relatively short rigid cylinders with the aspect ratio in the range $2 \lesssim \omega \lesssim 20$.[42] In our study, the parameters $a = 0.71\sigma$ and $b = 0.32\sigma$ were augmented by 0.5σ to take into account the finite size of LJ atoms, which gives the aspect ratio $\omega \approx 3.04$ that was used for the comparative analysis described below.

We first plot the rotational autocorrelation function of the unit vector $\mathbf{e}_1$ along the major axis of the rod-shaped particle $\langle \mathbf{e}_1(0)\cdot\mathbf{e}_1(t)\rangle$ in Figure 4. As expected, the rotational diffusion is

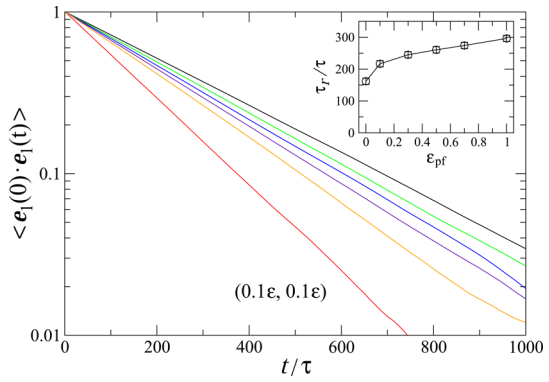

Figure 4. Time dependence of the correlation function $\langle \mathbf{e}_1(0)\cdot\mathbf{e}_1(t)\rangle$ for particles with surface energies $(0.1\varepsilon, 0.1\varepsilon)$, $(1.0\varepsilon, 0.1\varepsilon)$, $(1.0\varepsilon, 0.3\varepsilon)$, $(1.0\varepsilon, 0.5\varepsilon)$, $(1.0\varepsilon, 0.7\varepsilon)$, and $(1.0\varepsilon, 1.0\varepsilon)$ from left to right. The rotational relaxation time τ_r is shown in the inset as a function of the surface energy ε_{pf}. The data point at $\varepsilon_{pf} = 0$ is for a uniformly nonwetting particle.

enhanced for the uniformly nonwetting particle and for Janus particles with lower surface energy at the nonwetting end. It can be observed from Figure 4 that the data for different surface energies can be well described by the exponential decay

$$\langle \mathbf{e}_1(0)\cdot\mathbf{e}_1(t)\rangle = e^{-t/\tau_r} \tag{5}$$

where τ_r is the rotational relaxation time scale, and the corresponding rotational diffusion coefficient is given by $1/(2\tau_r)$.[29] The inset in Figure 4 shows the variation of τ_r as a function of the surface energy at the nonwetting end of the particle. It can be seen that the rotational relaxation time gradually varies between bounds determined by the limiting cases of uniformly wetting and nonwetting particles. The same data for τ_r are listed in Table 2. We comment that the effect of the particle shape, rod-like versus spherical, on rotational diffusion is evident from the results reported in Figure 4 in the present study and Figure 4 in ref 26. Namely, in the case of rod-shaped particles, the relaxation time associated with rotation of the unit vector $\mathbf{e}_1$ is larger by a factor of ∼1.5−3 for the same particle mass, surface wettability, fluid density, and temperature.[26]

Another way to quantify the rotational diffusion is to compute the average mean square *angular* displacement during the time interval t as follows

$$\langle \Delta\vec{\varphi}^2(t)\rangle = \frac{1}{N}\sum_{i=1}^{N} |\vec{\varphi}_i(t_0 + t) - \vec{\varphi}_i(t_0)|^2 = 4D_r t \tag{6}$$

where D_r is the rotational diffusion coefficient and $\vec{\varphi}(t)$ is the total angular displacement vector defined by

$$\vec{\varphi}(t) = \int_0^t \Delta\vec{\varphi}(t')\, dt' \tag{7}$$

with the magnitude of $\Delta\vec{\varphi}(t')$ given by $\cos^{-1}(\mathbf{e}_1(t)\cdot\mathbf{e}_1(t + t'))$, which is the rotation angle of the vector $\mathbf{e}_1$ during the time interval t'.[43,44] In this definition, the mean square angular displacement $\langle \Delta\vec{\varphi}^2(t)\rangle$ is unbounded and the diffusion coefficient is evaluated in the linear regime at large times.[43]

The results for the mean square angular displacement obtained from MD simulations are displayed in Figure 5 for

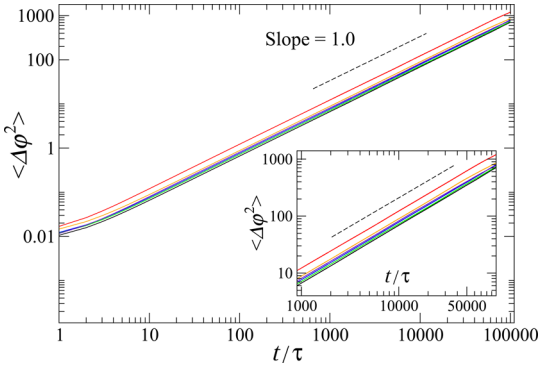

Figure 5. Mean square angular displacement $\langle \Delta\varphi^2\rangle$ (in units of rad^2) of the major axis (vector $\mathbf{e}_1$) for Janus and uniform particles with surface energies $(0.1\varepsilon, 0.1\varepsilon)$, $(1.0\varepsilon, 0.1\varepsilon)$, $(1.0\varepsilon, 0.3\varepsilon)$, $(1.0\varepsilon, 0.5\varepsilon)$, $(1.0\varepsilon, 0.7\varepsilon)$, and $(1.0\varepsilon, 1.0\varepsilon)$ from top to bottom. The dashed line with slope 1 is included as a reference. The inset shows an enlarged view of the same data at $t \geqslant 10^3\tau$.

uniform and Janus particles. It is clearly seen that Janus particles with larger wettability contrast diffuse faster, and their angular displacements are greater (smaller) than that of uniformly wetting (nonwetting) particles. The values of the rotational diffusion coefficient obtained from the linear fit to eq 6 are listed in Table 2 along with the prediction of eq 4. Thus, we conclude that both methods of evaluation of the diffusion

Table 2. Diffusion Coefficients for Uniformly Wetting and Nonwetting Particles as Well as Janus Particles with the Indicated Wettability Contrast[a]

$\varepsilon_{pf}/\varepsilon$	(1.0, 1.0)	(0.1, 0.1)	(1.0, 0.7)	(1.0, 0.5)	(1.0, 0.3)	(1.0, 0.1)	ref 42
$D_\perp\tau\sigma^{-2}$	0.0149	0.0242	0.0159	0.0165	0.0171	0.0179	0.0146
$D_\parallel\tau\sigma^{-2}$	0.0177	0.0291	0.0186	0.0197	0.0203	0.0209	0.0174
$D_t\tau\sigma^{-2}$	0.0158	0.0258	0.0168	0.0176	0.0182	0.0189	0.0155
$D_r\tau$	0.00176	0.00312	0.00185	0.00197	0.00202	0.00229	0.00122
τ_r/τ	296.3	161.9	274.3	260.6	245.1	216.8	
$\tau/2\tau_r$	0.00169	0.00309	0.00182	0.00192	0.00204	0.00231	

[a]The following parameters were evaluated from the fit to the MD data: $D_\perp$ using eq 9, $D_\parallel$ using eq 8, $D_t = (2D_\perp + D_\parallel)/3$, D_r using eq 6, τ_r using eq 5. The data in the last column were computed using eqs 2−4 from ref 42. Typical error bars are $6 \times 10^{-4}\tau\sigma^{-2}$.

DOI: 10.1021/acs.jpcb.7b03720
J. Phys. Chem. B 2017, 121, 7133−7139

coefficient, i.e., D_r from eq 6 and $1/(2\tau_r)$ from eq 5, give consistent results. However, we find that the value of the diffusion coefficient for a uniformly wetting particle is significantly larger than the analytical prediction of eq 4, possibly due to finite slip at the particle surface in MD simulations. It should be noted that a similar discrepancy between the prediction of eq 4 and MD results for the rotational diffusion of a carbon nanotube in a LJ fluid was recently reported by Cao and Dong.[45]

The mean square displacement in the directions parallel and perpendicular to the main axis of the uniformly wetting particle ($\varepsilon_{pf} = 1.0\varepsilon$) as well as its total mean square displacement are presented in Figure 6. As is evident, all curves have a unit slope

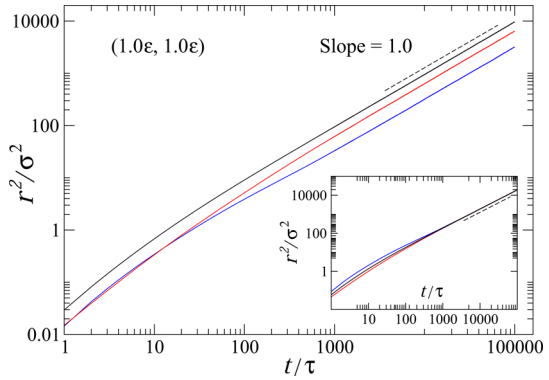

Figure 6. Mean square displacement in the direction parallel (blue curve) and perpendicular (red curve) to the major axis of the uniformly wetting rod with $\varepsilon_{pf} = 1.0\varepsilon$. The black curve denotes the total mean square displacement as a function of time. The straight dashed line with unit slope is plotted for reference. The inset shows the same data multiplied by different factors $6r_{\parallel}^2$, $3r_{\perp}^2$, and $2r_t^2$ (see text for details).

at large times but with different proportionality coefficients. By definition, the translational diffusion coefficient is a combination of parallel and perpendicular diffusion coefficients, i.e., $D_t = (2D_\perp + D_\parallel)/3$. To facilitate comparison, the data for the parallel, perpendicular, and total mean square displacements were multiplied by factors of 6, 3, and 2, respectively, and replotted in the inset of Figure 6. It can be observed that diffusion in the direction parallel to the major axis is faster than that in the perpendicular direction at $t \lesssim 500\tau$, while at larger times diffusion becomes isotropic as the orientation of the vector $\mathbf{e}_1$ is decorrelated (see Table 2). As shown in Figure 7, the same trends were observed for uniformly nonwetting and Janus particles. We also note that the gradual crossover from short-time anisotropic to long-time isotropic diffusion was observed for isolated ellipsoidal particles in water.[46]

In our analysis, the translational diffusion coefficients in the directions parallel and perpendicular to the major axis of a particle (along the vector $\mathbf{e}_1$) were evaluated using the following equations

$$\Delta r_{\parallel}^2(t) = \langle((\mathbf{r}(t_0 + t) - \mathbf{r}(t_0))\cdot\mathbf{e}_1(t_0))^2\rangle = 2D_{\parallel}t \quad (8)$$

$$\Delta r_{\perp}^2(t) = \langle|(\mathbf{r}(t_0 + t) - \mathbf{r}(t_0)) \times \mathbf{e}_1(t_0)|^2\rangle = 4D_{\perp}t \quad (9)$$

where t_0 is the reference time and the brackets $\langle..\rangle$ indicate averaging over all t_0. Equations 8 and 9 were used to fit the data shown in Figures 6 and 7 in the range $20\tau \lesssim t \lesssim \tau_r$. The results from numerical simulations and theoretical predictions of eqs 2−4 are reported in Table 2. It can be observed that, in the case

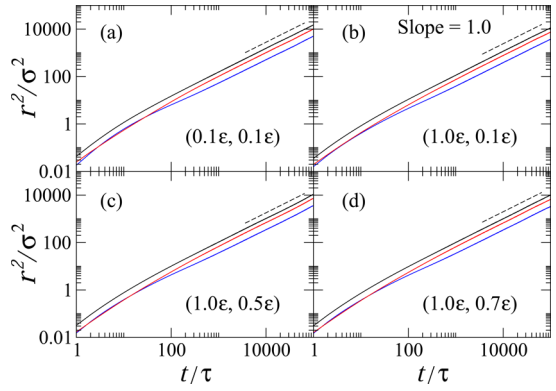

Figure 7. Averaged mean square displacements in the direction parallel (blue curves) and perpendicular (red curves) to the main axis of (a) a uniformly nonwetting particle with $\varepsilon_{pf} = 0.1\varepsilon$ and Janus particles with surface energies (b) $(1.0\varepsilon, 0.1\varepsilon)$, (c) $(1.0\varepsilon, 0.5\varepsilon)$, and (d) $(1.0\varepsilon, 0.7\varepsilon)$. The total mean square displacement is indicated by black curves. The dashed lines show unit slope.

of a uniformly wetting particle, the values of the diffusion coefficients obtained from the particle trajectory agree well with predictions of ref 42. We comment that this agreement might be coincidental because of the no-slip boundary condition assumed in derivation of eqs 2−4, while in MD simulations the local slip length at the particle's surface is relatively large even for the uniformly wetting case (see Table 1). Generally, the data in Table 2 follow the same trend; namely, the diffusion coefficients are largest (smallest) for uniformly nonwetting (wetting) particles, and the diffusion is enhanced for Janus particles with less wetting surfaces. The same behavior was reported for spherical Janus and uniform particles in the previous MD study.[26]

We next discuss more subtle aspects of the rotational dynamics arising due to the wettability contrast and asymmetrical shape of particles. The time dependence of the correlation function $\langle\mathbf{e}_1(0)\cdot\mathbf{e}_1(t)\rangle$, shown in Figure 4, provides an estimate of the rotational relaxation time scale τ_r, but it does not describe the relative motion of the wetting and nonwetting ends. From the analysis of particle trajectories, we computed the total length of paths traveled by the centers of the wetting and nonwetting half-sides separately. As expected, the lengths of such trajectories will be on average the same for uniformly wetting and nonwetting particles (data not shown). We also comment that the mean square displacements of the centers of wetting and nonwetting ends will also approach the same values at long times because they are determined by the displacement of the particle's center of mass. In contrast, as shown in Figure 8, the center of the nonwetting end follows a longer trajectory than the center of the wetting end of a Janus particle. The maximum difference in length of the trajectories is about $2.2 \times 10^3\sigma$ at $t = 3 \times 10^5\tau$ for the Janus particle with the maximum wettability contrast of $(1.0\varepsilon, 0.1\varepsilon)$. Correspondingly, the relative difference in this case is about 2%. These results demonstrate that, during diffusive motion of Janus particles, the nonwetting end "effectively" rotates around the wetting end. In other words, the center of rotation is displaced along the main axis toward the wetting end of the Janus particle.

Another peculiar feature of the diffusive motion of Janus particles is the correlation between translation and rotation due to asymmetric wetting.[26] When, due to thermal fluctuations, a Janus particle acquires a translational velocity in a certain direction, its nonwetting end will tend to rotate toward the

DOI: 10.1021/acs.jpcb.7b03720
J. Phys. Chem. B 2017, 121, 7133−7139

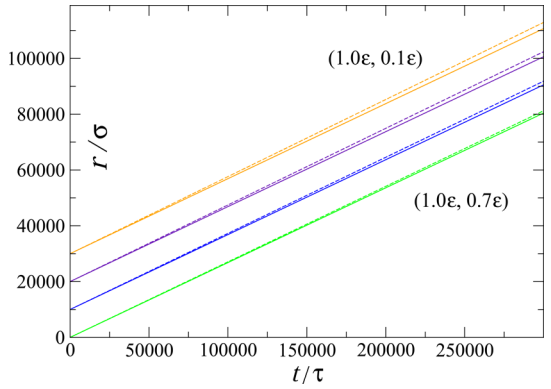

Figure 8. Total displacement, r/σ, of the centers of nonwetting (dashed lines) and wetting (solid lines) ends of Janus particles with surface energies $(1.0\varepsilon, 0.1\varepsilon)$, $(1.0\varepsilon, 0.3\varepsilon)$, $(1.0\varepsilon, 0.5\varepsilon)$, and $(1.0\varepsilon, 0.7\varepsilon)$ from top to bottom. The data for the first three cases are displaced vertically for clarity.

displacement to reduce drag. This effect can be quantified via the average rotation angle of the major axis along the displacement vector of the center of mass. We first consider the displacement vector of the center of mass $\Delta\mathbf{r}$ during a time interval t and then estimate the difference between the angles that vectors $\mathbf{e}_1(0)$ and $\mathbf{e}_1(t)$ make with respect to $\Delta\mathbf{r}$. In Figure 9, the rotation angle averaged over particle trajectories is

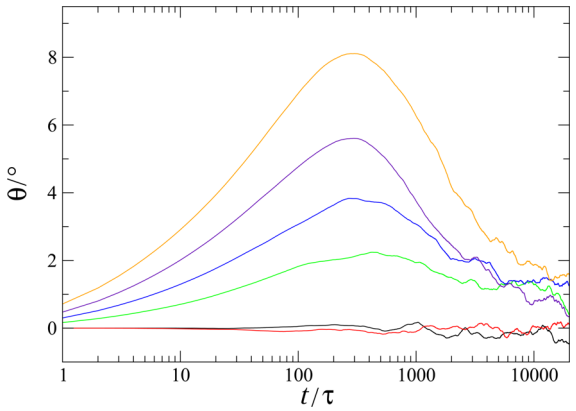

Figure 9. Angle of rotation of the vector $\mathbf{e}_1$ along the displacement vector of the center of mass of Janus particles with the wettability contrast $(1.0\varepsilon, 0.1\varepsilon)$, $(1.0\varepsilon, 0.3\varepsilon)$, $(1.0\varepsilon, 0.5\varepsilon)$, and $(1.0\varepsilon, 0.7\varepsilon)$ from top to bottom. The time dependence of the rotation angle for uniformly wetting (nonwetting) particles is denoted by black (red) curves.

plotted as a function of time for Janus and uniformly wetting particles. It can be seen that Janus particles indeed preferentially rotate along the displacement, and the maximum rotation angle is attained at intermediate times that roughly correspond to the rotational relaxation time scales τ_r (listed in Table 2). Interestingly, the maximum values of the rotation angle shown in Figure 9 are very close to the values reported in Figure 7 in ref 26 for spherical Janus particles with the same wettability contrast. However, the maximum rotation of rod-shaped Janus particles occurs at larger times than for spherical Janus particles due to the larger moment of inertia in the former case. Finally, as shown in Figure 9, the effect of correlated rotation is absent for uniformly wetting and nonwetting particles.

IV. CONCLUSIONS

In this paper, molecular dynamics simulations were performed to investigate the diffusive dynamics of Janus rod-shaped particles in an explicit solvent. We considered the limit of low dilution where interaction between particles can be neglected. The Janus particle was modeled as a rigid body where atoms are fixed at the vertices of adjacent hexagons and form a rod with an aspect ratio of about 3. The interaction energy between fluid monomers and particles' atoms was set to different values on both half-sides of a Janus particle. Two limiting cases of uniformly wetting and nonwetting particles were also considered for reference.

It was shown that both rotational and translational diffusion are enhanced for Janus particles with lower average wettability, while the largest (smallest) values of the corresponding diffusion coefficients were obtained for uniformly nonwetting (wetting) particles. Moreover, the estimates of the diffusion coefficients for displacement of the center of mass in the direction perpendicular and parallel to the major axis agree well with theoretical predictions in the case of a uniformly wetting particle. The numerical analysis of the particle trajectories revealed that the effective center of rotation of Janus particles is displaced along the major axis toward the wetting end. Finally, the results of our MD simulations indicate an unusual feature of the diffusive motion of Janus particles; namely, the nonwetting end of the Janus particle is rotated on average along the displacement vector of the center of mass in order to reduce the friction force from the surrounding fluid. Interestingly, the maximum value of the rotation angle for a given wettability contrast of rod-shaped particles is very close to the values reported in our previous study on diffusion of spherical Janus particles.[26]

AUTHOR INFORMATION

Corresponding Author

*E-mail: nikolai.priezjev@wright.edu. Phone: (937) 775-3214.

ORCID

Nikolai V. Priezjev: 0000-0002-4611-3479

Notes

The authors declare no competing financial interest.

ACKNOWLEDGMENTS

Financial support from the National Science Foundation (CBET-1033662 and CNS-1531923) is gratefully acknowledged. The study has been in part funded by the Russian Academic Excellence Project "5-100". Computational work in support of this research was performed at Michigan State University's High Performance Computing Facility and the Ohio Supercomputer Center. The molecular dynamics simulations were conducted using the LAMMPS numerical code developed at Sandia National Laboratories.[30]

REFERENCES

(1) Busseron, E.; Ruff, Y.; Moulin, E.; Giuseppone, N. Supramolecular self-assemblies as functional nanomaterials. *Nanoscale* **2013**, *5*, 7098.

(2) Guo, R.; Mao, J.; Xie, X.-M.; Yan, L.-T. Predictive supracolloidal helices from patchy particles. *Sci. Rep.* **2014**, *4*, 7021.

(3) Ma, C.; Wu, H.; Huang, Z.-H.; Guo, R.-H.; Hu, M.-B.; Kubel, C.; Yan, L.-T.; Wang, W. A filled-honeycomb-structured crystal formed by self-assembly of a Janus polyoxometalate-silsesquioxane (POM-POSS) co-cluster. *Angew. Chem., Int. Ed.* **2015**, *54*, 15699.

DOI: 10.1021/acs.jpcb.7b03720
J. Phys. Chem. B 2017, 121, 7133−7139

(4) Lattuada, M.; Hatton, T. A. Synthesis, properties and applications of Janus nanoparticles. *Nano Today* **2011**, *6*, 286.
(5) Xu, K.; Guo, R.; Dong, B.; Yan, L.-T. Directed self-assembly of Janus nanorods in binary polymer mixture: towards precise control of nanorod orientation relative to interface. *Soft Matter* **2012**, *8*, 9581.
(6) Li, W.; Dong, B.; Yan, L.-T. Janus nanorods in shearing-to-relaxing polymer blends. *Macromolecules* **2013**, *46*, 7465.
(7) Sacanna, S.; Pine, D. J.; Yi, G.-R. Engineering shape: the novel geometries of colloidal self-assembly. *Soft Matter* **2013**, *9*, 8096.
(8) Rogers, W. B.; Shih, W. M.; Manoharan, V. N. Using DNA to program the self-assembly of colloidal nanoparticles and microparticles. *Nature Reviews Materials* **2016**, *1*, 16008.
(9) Ould-Kaddour, F.; Levesque, D. Molecular-dynamics investigation of tracer diffusion in a simple liquid: Test of the Stokes-Einstein law. *Phys. Rev. E: Stat. Phys., Plasmas, Fluids, Relat. Interdiscip. Top.* **2000**, *63*, 011205.
(10) Schmidt, J. R.; Skinner, J. L. Hydrodynamic boundary conditions, the Stokes-Einstein law, and long-time tails in the Brownian limit. *J. Chem. Phys.* **2003**, *119*, 8062.
(11) Lee, S. H.; Kapral, R. Friction and diffusion of a Brownian particle in a mesoscopic solvent. *J. Chem. Phys.* **2004**, *121*, 11163.
(12) Schmidt, J. R.; Skinner, J. L. Brownian motion of a rough sphere and the Stokes-Einstein law. *J. Phys. Chem. B* **2004**, *108*, 6767.
(13) Ould-Kaddour, F.; Levesque, D. Diffusion of nanoparticles in dense fluids. *J. Chem. Phys.* **2007**, *127*, 154514.
(14) Li, Z. Critical particle size where the Stokes-Einstein relation breaks down. *Phys. Rev. E* **2009**, *80*, 061204.
(15) Shin, H. K.; Kim, C.; Talkner, P.; Lee, E. K. Brownian motion from molecular dynamics. *Chem. Phys.* **2010**, *375*, 316.
(16) Chakraborty, D. Velocity autocorrelation function of a Brownian particle. *Eur. Phys. J. B* **2011**, *83*, 375.
(17) Ishii, Y.; Ohtori, N. Molecular insights into the boundary conditions in the Stokes-Einstein relation. *Phys. Rev. E: Stat. Phys., Plasmas, Fluids, Relat. Interdiscip. Top.* **2016**, *93*, 050104.
(18) Alder, B.; Wainwright, T. Decay of the velocity autocorrelation function. *Phys. Rev. A: At., Mol., Opt. Phys.* **1970**, *1*, 18.
(19) Huang, K.; Szlufarska, I. Effect of interfaces on the nearby Brownian motion. *Nat. Commun.* **2015**, *6*, 8558.
(20) Felderhof, B. U. Effect of the wall on the velocity autocorrelation function and long-time tail of Brownian motion. *J. Phys. Chem. B* **2005**, *109*, 21406.
(21) Swan, J. W.; Khair, A. S. On the hydrodynamics of 'slip−stick' spheres. *J. Fluid Mech.* **2008**, *606*, 115.
(22) Willmott, G. R. Dynamics of a sphere with inhomogeneous slip boundary conditions in Stokes flow. *Phys. Rev. E* **2008**, *77*, 055302.
(23) Willmott, G. R. Slip-induced dynamics of patterned and Janus-like spheres in laminar flows. *Phys. Rev. E* **2009**, *79*, 066309.
(24) Sun, Q.; Klaseboer, E.; Khoo, B. C.; Chan, D. Y. C. Stokesian dynamics of pill-shaped Janus particles with stick and slip boundary conditions. *Phys. Rev. E* **2013**, *87*, 043009.
(25) Rezvantalab, H.; Drazer, G.; Shojaei-Zadeh, S. Molecular simulation of translational and rotational diffusion of Janus nanoparticles at liquid interfaces. *J. Chem. Phys.* **2015**, *142*, 014701.
(26) Kharazmi, A.; Priezjev, N. V. Diffusion of a Janus nanoparticle in an explicit solvent: A molecular dynamics simulation study. *J. Chem. Phys.* **2015**, *142*, 234503.
(27) Rezvantalab, H.; Shojaei-Zadeh, S. Tilting and tumbling of Janus nanoparticles at sheared interfaces. *ACS Nano* **2016**, *10*, 5354.
(28) Archereau, A. Y. M.; Hendy, S. C.; Willmott, G. R. Molecular dynamics simulations of Janus particle dynamics in uniform flow. arXiv:1606.02850, 2016.
(29) Wang, A.; Dimiduk, T. G.; Fung, J.; Razavi, S.; Kretzschmar, I.; Chaudhary, K.; Manoharan, V. N. Using the discrete dipole approximation and holographic microscopy to measure rotational dynamics of non-spherical colloidal particles. *J. Quant. Spectrosc. Radiat. Transfer* **2014**, *146*, 499.
(30) Plimpton, S. J. Fast parallel algorithms for short-range molecular dynamics. *J. Comput. Phys.* **1995**, *117*, 1.
(31) Allen, M. P.; Tildesley, D. J. *Computer Simulation of Liquids*; Clarendon: Oxford, U.K., 1987.
(32) Priezjev, N. V.; Darhuber, A. A.; Troian, S. M. Slip behavior in liquid films on surfaces of patterned wettability: Comparison between continuum and molecular dynamics simulations. *Phys. Rev. E* **2005**, *71*, 041608.
(33) Priezjev, N. V. Molecular diffusion and slip boundary conditions at smooth surfaces with periodic and random nanoscale textures. *J. Chem. Phys.* **2011**, *135*, 204704.
(34) Priezjev, N. V. Rate-dependent slip boundary conditions for simple fluids. *Phys. Rev. E* **2007**, *75*, 051605.
(35) Priezjev, N. V. Effect of surface roughness on rate-dependent slip in simple fluids. *J. Chem. Phys.* **2007**, *127*, 144708.
(36) Priezjev, N. V. Relationship between induced fluid structure and boundary slip in nanoscale polymer films. *Phys. Rev. E* **2010**, *82*, 051603.
(37) Hu, H.; Bao, L.; Priezjev, N. V.; Luo, K. Identifying two regimes of slip of simple fluids over smooth surfaces with weak and strong wall-fluid interaction energies. *J. Chem. Phys.* **2017**, *146*, 034701.
(38) Priezjev, N. V.; Troian, S. M. Influence of periodic wall roughness on the slip behaviour at liquid/solid interfaces: molecular-scale simulations versus continuum predictions. *J. Fluid Mech.* **2006**, *554*, 25.
(39) Niavarani, A.; Priezjev, N. V. Modeling the combined effect of surface roughness and shear rate on slip flow of simple fluids. *Phys. Rev. E* **2010**, *81*, 011606.
(40) Chen, W.; Zhang, R.; Koplik, J. Velocity slip on curved surfaces. *Phys. Rev. E* **2014**, *89*, 023005.
(41) Guo, L.; Chen, S.; Robbins, M. O. Slip boundary conditions over curved surfaces. *Phys. Rev. E: Stat. Phys., Plasmas, Fluids, Relat. Interdiscip. Top.* **2016**, *93*, 013105.
(42) Tirado, M. M.; Martinez, C. L.; de la Torre, J. G. Comparison of theories for the translational and rotational diffusion coefficients of rod-like macromolecules. Application to short DNA fragments. *J. Chem. Phys.* **1984**, *81*, 2047.
(43) Kammerer, S.; Kob, W.; Schilling, R. Dynamics of the rotational degrees of freedom in a supercooled liquid of diatomic molecules. *Phys. Rev. E: Stat. Phys., Plasmas, Fluids, Relat. Interdiscip. Top.* **1997**, *56*, 5450.
(44) Edmond, K. V.; Elsesser, M. T.; Hunter, G. L.; Pine, D. J.; Weeks, E. R. Decoupling of rotational and translational diffusion in supercooled colloidal fluids. *Proc. Natl. Acad. Sci. U. S. A.* **2012**, *109*, 17891.
(45) Cao, B.-Y.; Dong, R.-Y. Molecular dynamics calculation of rotational diffusion coefficient of a carbon nanotube in fluid. *J. Chem. Phys.* **2014**, *140*, 034703.
(46) Han, Y.; Alsayed, A. M.; Nobili, M.; Zhang, J.; Lubensky, T. C.; Yodh, A. G. Brownian motion of an ellipsoid. *Science* **2006**, *314*, 626.

DOI: 10.1021/acs.jpcb.7b03720
J. Phys. Chem. B 2017, 121, 7133−7139